NANO LETTERS

Letter

pubs.acs.org/NanoLett

Evidence for Defect-Mediated Tunneling in Hexagonal Boron Nitride-Based Junctions

U. Chandni,*[,†] K. Watanabe,[‡] T. Taniguchi,[‡] and J. P. Eisenstein[†]

[†]Institute for Quantum Information and Matter, Department of Physics, California Institute of Technology, 1200 East California Boulevard, Pasadena, California 91125, United States

[‡]National Institute for Materials Science, 1-1 Namiki, Tsukuba, Ibaraki 305-0044, Japan

Supporting Information

ABSTRACT: We investigate electron tunneling through atomically thin layers of hexagonal boron nitride (hBN). Metal (Cr/Au) and semimetal (graphite) counter-electrodes are employed. While the direct tunneling resistance increases nearly exponentially with barrier thickness as expected, the thicker junctions also exhibit clear signatures of Coulomb blockade, including strong suppression of the tunnel current around zero bias and step-like features in the current at larger biases. The voltage separation of these steps suggests that single-electron charging of nanometer-scale defects in the hBN barrier layer are responsible for these signatures. We find that annealing the metal−hBN−metal junctions removes these defects and the Coulomb blockade signatures in the tunneling current.

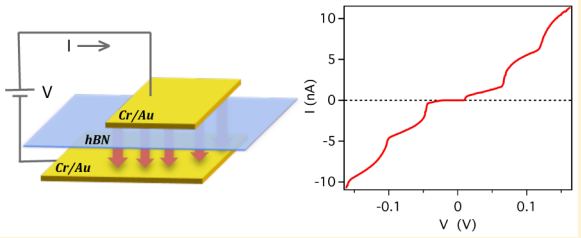

KEYWORDS: *Tunneling, hexagonal boron nitride (hBN), hBN defects, graphite, coulomb blockade, annealing*

Van der Waals heterostructures, where layered stacks of two-dimensional materials are embedded in precisely desired patterns, have gained immense attention in recent times.[1,2] Such tailor-made structures of graphene, hexagonal boron nitride (hBN), metal dichalcogenides, and other 2D materials offer exotic device geometries to explore new physics. Tunnel junctions with an atomically thin insulator barrier sandwiched between atomic layers of 2D materials form an interesting structure in this respect. In conventional two-dimensional semiconductor double layer structures, tunneling has shown remarkable features, including resonant tunneling, Coulomb correlations at high magnetic fields, and Landau-level spectroscopy.[3−6] In the regime of 2D layered materials, hBN with a band gap of ∼5.9 eV[7] is an ideal candidate for an insulating barrier.[8] Recent studies on heterostructures with single and bilayer graphene as electrodes and hBN as the insulator have shown interesting features, including a very strong negative differential resistance (NDR).[9−12] In all of these transport studies hBN is assumed to be a benign element. However, from a materials perspective there have been extensive efforts to understand the underlying structure and defect mechanisms in thin layers of hBN, which can have important consequences on electrical transport.[13−15] Here we present detailed tunneling transport measurements on simple junctions consisting of metal or graphite electrodes separated by a thin hBN layer. Our results demonstrate that the hBN insulator can yield unexpected transport signatures suggestive of defect-mediated tunneling processes.

In a conventional metal−insulator−metal (M−I−M) junction, the tunnel current−voltage characteristic ($I-V$) is linear at low biases, with the tunneling resistance inversely proportional to sample area and exponentially dependent on the barrier thickness d. Our studies show that the $I-V$ with hBN as the barrier is distinct from such a simple behavior in various respects. Thinner barrier devices show a finite linear tunnel current at low biases and a roughly exponential dependence of the low bias resistance with d, complying with standard quantum mechanical tunneling, in agreement with previous reports.[9,12] However, in relatively thicker barrier devices, we find signatures of Coulomb blockade and single electron tunneling events. The signatures we observe in these presumably large area planar M−I−M junctions are strikingly similar to those seen in metallic islands and semiconductor quantum dots at low temperatures.[16]

We have primarily investigated tunnel junctions comprising Cr/Au-hBN-Cr/Au (see Figure 1a) with 2−6 atomic layers of hBN forming the insulating layer, beyond which tunnel current was unobservably low. The device fabrication begins by mechanically exfoliating hBN flakes on a Si/SiO_2 wafer. Figure 1b shows a typical hBN flake. These are further characterized by a combination of optical microscopy, atomic force microscopy, and Raman spectroscopy to determine the number of hBN atomic layers. We note that employing a Nomarski interference contrast microscope helps in identifying thinner layers of hBN, which have lower optical contrast than graphene. The hBN flake is then transferred to another Si/SiO_2 wafer previously patterned with narrow Cr/Au electrodes, shown as vertical gold lines in Figure 1c. We have used the dry transfer

Received: July 3, 2015
Revised: October 27, 2015
Published: October 28, 2015

DOI: 10.1021/acs.nanolett.5b02625
Nano Lett. 2015, 15, 7329−7333

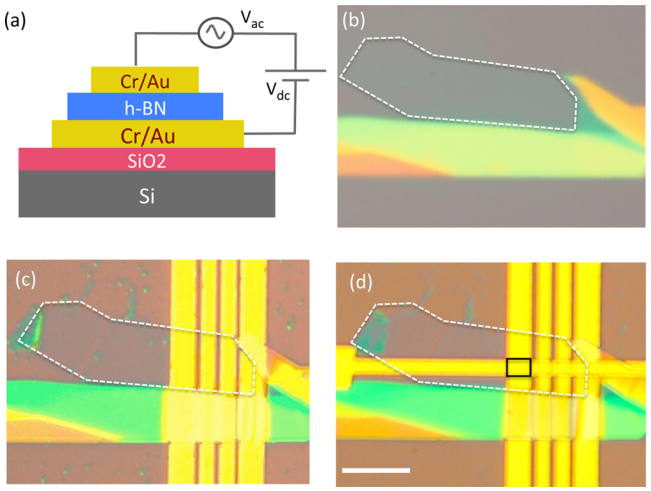

Figure 1. (a) Device structure for h-BN tunnel devices with Cr/Au electrodes. (b) An optical micrograph of a thin hBN flake. Dotted line shows the thin region of interest. (c) hBN flake transferred on to a set of bottom electrodes. (d) Tunnel device with the horizontal top electrode forming multiple tunnel junctions, one of which is marked as a box. Scale bar is 10 μm.

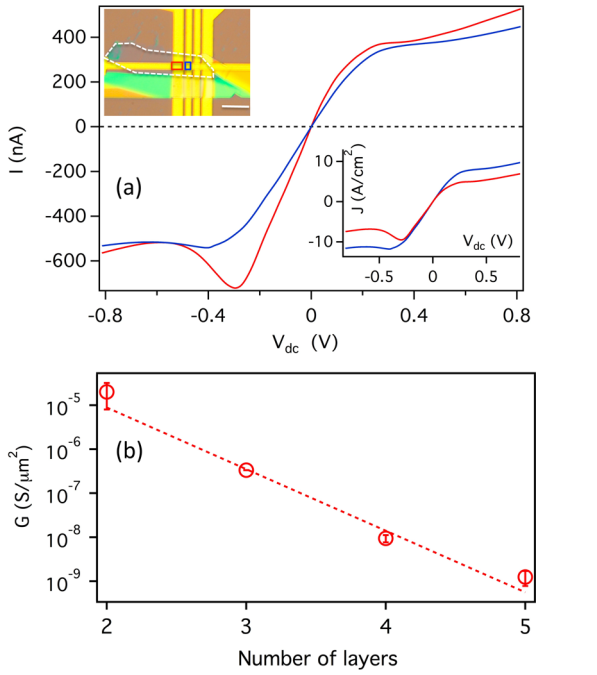

Figure 2. (a) Tunnel current (I) as a function of dc bias (V_{dc}) for a typical thin hBN (dotted line) device with ~3 layers. Two tunnel junctions are shown in the inset optical micrograph, with areas 3.8 × 2 μm^2 (red) and 2.3 × 2 μm^2 (blue). Scale bar is 10 μm. The inset graph shows the tunnel current density (J) for the two junctions as a function of bias. (b) Conductance per unit area G as a function of number of layers. Dotted line indicates an exponential fit.

method developed by Wang et al.[2] for all our devices. The top Cr/Au electrode (horizontal gold pad in Figure 1d) is then lithographically patterned. In all the devices, there are several bottom electrodes and one top electrode, thus forming multiple tunnel junctions (one out of four tunnel junctions in Figure 1d is indicated by the box) each of which can be measured in a four-terminal geometry. Typical junctions vary from 1.4 × 0.5 to 4 × 2 μm^2 in area. Detailed discussion on the fabrication steps and characterization of the hBN flakes can be found in the Supporting Information. The tunneling current I and differential conductance dI/dV in response to voltage excitation ($V = V_{dc}+V_{ac}$, with V_{ac} = 0.5 mV at 13 Hz) were recorded simultaneously. Three different batches of hBN crystals were used for the present study, and no qualitative differences were seen. In addition to junctions with Cr/Au electrodes, we have also examined graphite−hBN−graphite devices. All of the data were taken at T = 4.2 K.

We first focus on thinner hBN devices with ≲5 atomic layers (each layer being ~0.34 nm thick.[8]) Ten junctions (from four separate hBN flakes) with varying d and area A were tested. The I−V curves show an ohmic dependence at dc bias V_{dc} < ±100 mV in all the junctions tested. (At higher biases, the I−V characteristics show substantial nonlinearity. We will return to this later.) Figure 2a presents an optical-micrograph of a three atomic layer hBN device with junctions of varying area, along with I−V data from two of the junctions. At low bias voltages both junctions display a linear I−V. The lower inset to the figure shows that the current density $J = I/A$ for the two junctions is the same in the linear regime $|V_{dc}| \lesssim 100$ mV, as expected for a simple tunnel junction.

At low biases with negligible barrier deformation, the linear current density for a M−I−M junction[17] is

$$J \propto \exp\left(\frac{-2d\sqrt{2m^*\phi_B}}{\hbar}\right)V \qquad (1)$$

where ϕ_B is the tunnel barrier height and m^* is the effective mass. Figure 2b reveals that the low-bias tunneling conductance per unit area $G = J/V$ in our thinner barrier devices exhibits this basic exponential dependence. Not surprisingly, small variations in G among the various junctions with same d are observed, shown by error bars in Figure 2b. These variations might be due to lack of uniform contact with the gold electrodes. An estimate to the factor $m^*\phi_B$ can be obtained by fitting a simple exponential to the G vs d data. Assuming the effective mass to be 0.26m_0 for the conduction band edge in hBN,[18] we get ϕ_B = 3.3 eV. This seems reasonable given the presently unknown alignment of the ~5.9 eV hBN band gap relative to the Fermi level in the electrodes and the appropriate effective mass for an electron tunneling far from the hBN conduction and valence band edges.

We now turn to tunneling transport in samples with thicker hBN barrier layers (≥6 layers). Figure 3a shows a typical device with five tunnel junctions of area 1.4 × 0.5 μm^2. Here, we find large discrepancy in the quantitative values of the tunnel current density between the different junctions that are geometrically identical. While most of the junctions had a clear suppressed tunneling region around zero bias (green), some of the junctions also showed discrete steps in the I−V (red and blue). Figure 3b shows dI/dV as a function of V_{dc}. Consistent with the steps in I−V, periodic oscillations in dI/dV are seen with a voltage spacing ~60 mV. These features show very little dependence on magnetic field and persist in temperature up to about 77 K.

This zero-bias suppression and staircase pattern in I−V bear strong resemblance to Coulomb blockade features seen in metallic or semiconducting dots.[16] While the suppression of current around zero bias is a universal feature of Coulomb blockade, the Coulomb staircase constitutes a rather special case where the tunnel barriers that isolate the island from the leads are asymmetric (with unequal tunneling resistances and/

DOI: 10.1021/acs.nanolett.5b02625
Nano Lett. 2015, 15, 7329−7333

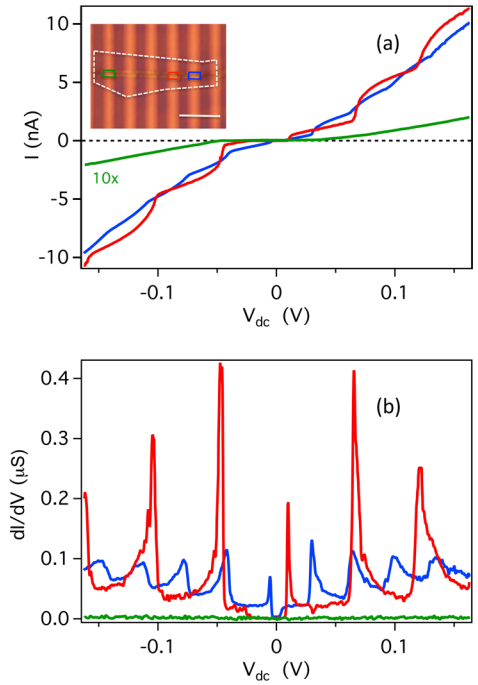

Figure 3. (a) Tunnel current (I) and (b) differential conductance (dI/dV) as a function of dc bias (V_{dc}) for a typical thick hBN device with ~6 layers. Green, blue, and red denote three junctions with area 1.4 × 0.5 μm^2 as shown in the inset. Scale bar is 5 μm.

or capacitances).[19,20] In such a scenario, an extra electron dwells in the island as the transmittance through one of the barriers is suppressed. The question here is, what acts as a dot or an island separated from the metal electrodes?

For the data shown in Figure 3b, the roughly 60 mV separation between the peaks in dI/dV suggests a Coulomb island whose net capacitance is on the order of $C \approx 2.6$ aF. This is roughly 4 orders of magnitude smaller than the capacitance between the tunneling electrodes. Indeed, modeling the Coulomb island as a disk of radius r midway between the two electrodes suggests $r \approx 3$ nm.

In conventional Coulomb blockade devices a characteristic dependence of the $I-V$ curve on an external gate potential (the so-called "diamond pattern") is generally observed. In contrast, the sharp features seen in our devices do not show any dependence on the voltage applied to the heavily doped Si substrate beneath the oxide layer on which the tunnel junctions are deposited. This is not surprising since the bottom electrode effectively screens the electric field resulting from a voltage applied to the Si substrate. Indeed, external electric fields arising from the substrate, or independent coplanar electrodes, cannot penetrate into the tunneling region by more than roughly the thickness $d \approx 2$ nm of the hBN layer. Thus, unless the Coulomb island is extremely close to the edge of the tunnel junction, no "diamond pattern" can be observed.

One possible candidate that complies with the small size of the island is the intrinsic defect in the hBN layer. In best quality hBN crystals, carbon and oxygen impurities can be as low as $10^{17}-10^{18}/cm^3$, which have been experimentally determined by secondary ion mass spectroscopy (SIMS) and cathode luminescence.[21] This would correspond to a minimum of 100 such defects in a 1 × 1 μm^2 area for a 1 nm thin sample of hBN. However, SIMS profile at various locations on a crystal often exhibit varying defect concentrations (at times exceeding $10^{18}/cm^3$), indicating an inhomogeneous carbon and oxygen impurity coverage. In addition, transmission electron microscopy (TEM) studies have revealed vacancies, interstitial defects, and ionized centers in hBN samples.[14,22,23] Recent reports of photoinduced doping in graphene on hBN substrates[24] and scanning tunneling microscopy studies of defects in exfoliated hBN[25] substantiates this picture. Importantly, defects and voids in hBN can even lead to interlayer bonding in contrast to few layer graphene sheets.[15] This suggests that defects can play a major role in tunneling transport as well, forming small isolated islands in the insulating matrix acting like quantum dots, where adding an extra electron costs energy. In many of our Cr/Au-based junctions the steps in $I-V$ were nearly periodic, indicative of a single charge center. We thus have two possible tunneling mechanisms: (1) conventional direct tunneling that scales with area and depends exponentially on the barrier thickness and (2) tunneling mediated by defects. The former is more pronounced in thinner samples, while the latter contributes to the sharp features in dI/dV in moderately thick samples where direct tunneling is weak.

In order to eliminate any possible influence of the electrode metal or the fabrication process, we have tested graphite–hBN–graphite devices as well. Device G1 consisted of three junctions with ~6 atomic layers of hBN. Here, the bottom graphite electrodes were fabricated by mechanical exfoliation followed by e-beam lithography and oxygen plasma etch to create multiple electrodes. The hBN flake was deposited on the bottom graphite electrodes, followed by the transfer and fabrication of a top graphite electrode. Graphite offers an atomically flat electrode surface for the tunnel junction. As can be seen from Figure 4a, we find very similar characteristics even in this case, with a blockaded region around zero bias and step-like characteristics in the $I-V$. Thus, a bad contact with the Au electrodes or the possibility of a Au dot in the hBN layers due to the fabrication procedure can be safely dismissed. In case of device G2, we have used a dry transfer pick-up method to avoid polymer residues in the tunnel junction region from the fabrication processes. Here the top graphite layer is used to pick up the hBN layer, and this graphite–hBN stack is deposited on the bottom graphite to form a clean junction. Device fabrication details can be found in the Supporting Information. The device under test had a four-layer hBN barrier and clearly exhibited step-like features in the $I-V$ (see Figure 4b), indicating that the polymer residues from the fabrication processes are not responsible for the Coulomb blockade-like features we observe. Note that the current is not fully blockaded in this device due to significant direct tunneling (see the inset to Figure 4b). Interestingly, although we observe step-like features in the graphite-based tunnel junctions bearing similarities to the Cr/Au-based junctions, a periodic staircase pattern similar to Figure 3b was not observed. This could be due to the presence of multiple defects with varying capacitances to the electrodes. There remains, of course, the possibility that graphite-based junctions have distinct tunneling characteristics not present in metal-based junctions.

In addition to probing the signatures of defects in charge transport, we also find that we can manipulate them by external means. To achieve this, we annealed some of the devices that showed significant Coulomb blockade features in an Ar/H_2 environment at 350 °C for 3–4 h. Figure 5 shows the results for one such Cr/Au-hBN-Cr/Au junction; similar results were obtained from other junctions as well. As the figure reveals, the pristine sample, for which the hBN layer was sufficiently thick

DOI: 10.1021/acs.nanolett.5b02625
Nano Lett. 2015, 15, 7329–7333

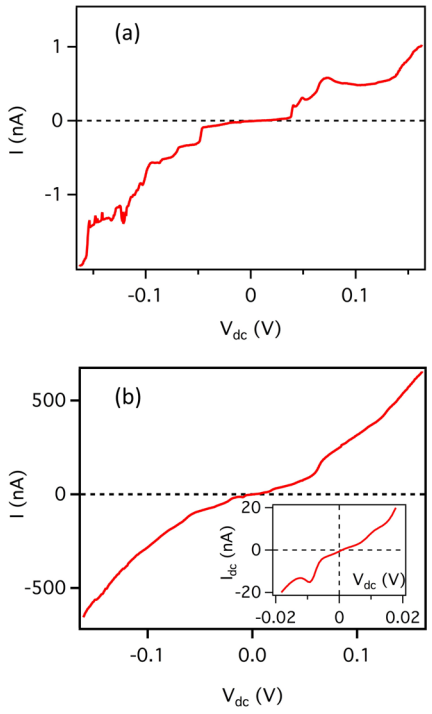

Figure 4. (a) Tunneling $I-V$ for a graphite−hBN−graphite junction (Device G1), with an area 2 × 1.5 μm^2. Two other junctions showed similar characteristics. (b) Tunneling $I-V$ for a graphite−hBN−graphite stack (Device G2) made via a dry transfer pick-up method. The device consisted of four atomic layers of hBN and an area of ∼4 × 6 μm^2. Inset shows the $I-V$ around zero bias exhibiting a finite conductance, indicative of direct tunneling.

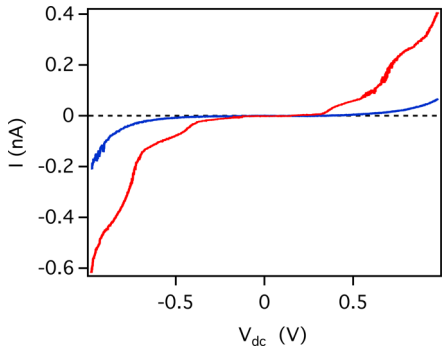

Figure 5. $I-V$ for a thick hBN barrier tunnel junction with Cr/Au electrodes, before (red) and after (blue) annealing in Ar−H_2 environment. Similar results were obtained for three more junctions in two sets of devices.

that no direct tunneling was expected or observed, showed pronounced Coulomb blockade and staircase features, with E_c ≈ 100 meV. After annealing, all signatures of single electron charging effects are absent. Only at relatively large bias, $|V_{dc}| \approx$ 0.6 V, does a significant tunneling current gradually appear. While four of the Cr/Au-hBN-Cr/Au junctions (in devices made from two different hBN flakes) exhibited similar drastic changes with annealing, the graphite−hBN−graphite device G2 fabricated via the dry transfer process did not exhibit any change on annealing. This could be due to subtle differences between the Cr/Au and graphite-based junctions, or due to the polymer residues present in the Cr/Au-based junctions, which are expected to be absent in the device G2 fabricated via the dry transfer process. We note that annealing exfoliated hBN flakes before transferring graphene onto them is considered an important step in achieving high mobilities for the graphene.[26] However, the microscopic mechanisms behind such improvements with annealing are still not fully clear. In bulk hBN, vacancy migration is expected to occur around 500 C.[27] Recent TEM studies on atomic layers of hBN have revealed grain boundaries, square−octagon (4|8) defects and pentagon−heptagon defects (5|7) in addition to vacancies and interstitials.[13,14] While experiments have revealed that 4|8 defects are mobile at about 800 C under e-beam irradiation,[14] 5|7 defects are expected to move to the boundary and stop or vanish.[28] Whether annealing cures some of the defects or mobilizes them will need a microscopic analysis using techniques like TEM and is beyond the scope of this work. Nevertheless, this indicates that the features have an intrinsic origin and may also be tuned via simple annealing steps.

We now return to the thin barrier devices at large bias voltages. Beyond the ohmic low bias region, the $I-V$ curves showed a pronounced nonmonotonic region, in many cases resembling an NDR feature as seen in Figure 2a. Figure 6

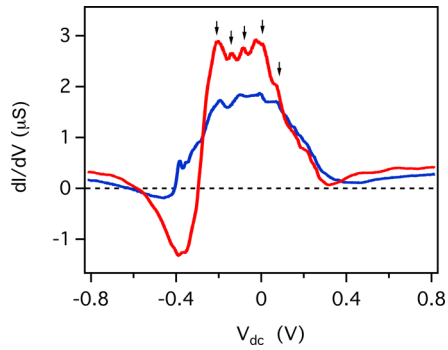

Figure 6. Differential conductance dI/dV vs V_{dc} for the thin barrier device shown in Figure 2a. Red and blue denote the two junctions shown in the inset of Figure 2a.

shows the differential conductance dI/dV as a function of V_{dc} for the two junctions discussed in Figure 2a, where the nonohmic behavior can be seen beyond $V_{dc} \approx 0.2-0.3$ V. While the red curve shows a clear NDR region in the negative voltage side, the effect is less pronounced in the positive side and for the blue curve. In a typical M−I−M junction at very high biases, the current across the junction is dominated by Fowler−Nordheim tunneling where the barrier is essentially triangular and the current density increases exponentially with the applied bias.[8] The voltage range probed here is believed to be below this regime, as our analysis of the low bias resistance gives the barrier height to be $\phi_B \approx 3.3$ eV and the hBN band gap is known to be ∼5.9 eV. However, the band alignment in the heterostructures employing such layered materials and metals remains unknown as discussed earlier. In recent studies, NDR signatures were observed in single and bilayer graphene based heterostructures, which were attributed to resonant tunneling via momentum conservation when the energy bands of the top and bottom graphene layers were aligned.[11,12] However, we find similar $I-V$ curves in simple M−I−M junctions here, albeit with peak to valley ratios lower than in graphene based devices. Interestingly, the only common feature in all these devices is the hBN barrier layer. The origin of these nonohmic features remains ambiguous. Finally, we also observe several weak peaks at regular intervals in the dI/dV (marked with arrows), in many of the samples. These may be due to defect-mediated single

DOI: 10.1021/acs.nanolett.5b02625
Nano Lett. 2015, 15, 7329−7333

electron charging events adding to the much larger direct tunnel current.

In conclusion, we have reported tunneling transport experiments on simple tunnel junctions consisting of metal (or graphite) electrodes separated by hexagonal boron nitride barrier layers. For thin hBN layers, direct tunneling, with reasonable area and barrier width scaling is observed at low biases, while unexplained nonlinear effects are seen at higher biases. In many of our devices, we observe step-like features in $I-V$ indicative of single electron charging events. We suggest that the intrinsic defects in the hBN insulator act as quantum dots sandwiched between metal (or graphite) electrodes and contribute to the observed tunneling characteristics. In devices with thin layers of hBN as the barrier, these features may appear along with dominant direct tunneling. These defect states, and hence the tunneling transport, can be altered through a simple annealing process.

■ ASSOCIATED CONTENT

Supporting Information

The Supporting Information is available free of charge on the ACS Publications website at DOI: 10.1021/acs.nanolett.5b02625.

Characterization of the hBN flakes using optical, AFM, and Raman measurements and details of device fabrication (PDF)

■ AUTHOR INFORMATION

Corresponding Author

*E-mail: chandniu@caltech.edu.

Notes

The authors declare no competing financial interest.

■ ACKNOWLEDGMENTS

We thank J. Petta, J. Velasco Jr., and D. Wong for useful discussions. Special thanks to G. Rossman for the use of his Raman spectroscopy facility. Atomic force microscopy was done at the Molecular Materials Research Center of the Beckman Institute at the California Institute of Technology. This work was supported by the Institute for Quantum Information and Matter, an NSF Physics Frontiers Center with support of the Gordon and Betty Moore Foundation through Grant No. GBMF1250.

■ REFERENCES

(1) Geim, A. K.; Grigorieva, I. V. *Nature* **2013**, *499*, 419−425.
(2) Wang, L.; Meric, I.; Huang, P. Y.; Gao, Q.; Gao, Y.; Tran, H.; Taniguchi, T.; Watanabe, K.; Campos, L. M.; Muller, D. A.; Guo, J.; Kim, P.; Hone, J.; Shepard, K. L.; Dean, C. R. *Science* **2013**, *342*, 614−617.
(3) Smoliner, J. *Semicond. Sci. Technol.* **1996**, *11*, 1−16.
(4) Eisenstein, J. P.; Pfeiffer, L. N.; West, K. W. *Appl. Phys. Lett.* **1991**, *58*, 1497−1499.
(5) Eisenstein, J. P.; Pfeiffer, L. N.; West, K. W. *Phys. Rev. Lett.* **1992**, *69*, 3804−3807.
(6) Brown, K. M.; Turner, N.; Nicholls, J. T.; Linfield, E. H.; Pepper, M.; Ritchie, D. A.; Jones, G. A. C. *Phys. Rev. B: Condens. Matter Mater. Phys.* **1994**, *50*, 15465−15468.
(7) Watanabe, K.; Taniguchi, T.; Kanda, H. *Nat. Mater.* **2004**, *3*, 404−409.
(8) Lee, G.-H.; Yu, Y.-J.; Lee, C.; Dean, C.; Shepard, K. L.; Kim, P.; Hone, J. *Appl. Phys. Lett.* **2011**, *99*, 243114.
(9) Britnell, L.; Gorbachev, R. V.; Jalil, R.; Belle, B. D.; Schedin, F.; Katsnelson, M. I.; Eaves, L.; Mozorov, S. V.; Mayorov, A. S.; Peres, N. M. R.; Castro Neto, A. H.; Leist, J.; Geim, A. K.; Ponomarenko, L. A.; Novoselov, K. S. *Nano Lett.* **2012**, *12*, 1707−1710.
(10) Britnell, L.; Gorbachev, R. V.; Geim, A. K.; Ponomarenko, L. A.; Mishchenko, A.; Greenaway, M. T.; Fromhold, T. M.; Novoselov, K. S.; Eaves, L. *Nat. Commun.* **2013**, *4*, 1794.
(11) Mishchenko, A.; Tu, J. S.; Cao, Y.; Gorbachev, R. V.; Wallbank, J. R.; Greenaway, M. T.; Morozov, V. E.; Morozov, S. V.; Zhu, M. J.; Wong, S. L.; Withers, F.; Woods, C. R.; Kim, Y.-J.; Watanabe, K.; Taniguchi, T.; Vdovin, E. E.; Makarovsky, O.; Fromhold, T. M.; Falko, V. I.; Geim, A. K.; Eaves, L.; Novoselov, K. S. *Nat. Nanotechnol.* **2014**, *9*, 808−813.
(12) Fallahazad, B.; Lee, K.; Kang, S.; Xue, J.; Larentis, S.; Corbet, C.; Kim, K.; Movva, H. C. P.; Taniguchi, T.; Watanabe, K.; Register, L. F.; Banerjee, S. K.; Tutuc, E. *Nano Lett.* **2015**, *15*, 428−433.
(13) Gibb, A. L.; Alem, N.; Chen, J.-H.; Erickson, K. J.; Ciston, J.; Gautam, A.; Linck, M.; Zettl, A. *J. Am. Chem. Soc.* **2013**, *135*, 6758−6761.
(14) Cretu, O.; Lin, Y.-C.; Suenaga, K. *Nano Lett.* **2014**, *14*, 1064−1068.
(15) Rasool, H. I.; Ophus, C.; Zettl, A. *Adv. Mater.* **2015**, *27*, 5771.
(16) Kouwenhoven, L. P.; Marcus, C. M.; McEuen, P. L.; Tarucha, S.; Westervelt, R. M.; Wingreen, N. S. *Proceedings of the NATO Advanced Study Institute on Mesoscopic Electron Transport* **1997**, 105−214.
(17) Simmons, J. G. *J. Appl. Phys.* **1963**, *34*, 1793.
(18) Xu, Y. N.; Ching, W. Y. *Phys. Rev. B: Condens. Matter Mater. Phys.* **1991**, *44*, 7787.
(19) Averin, D. V.; Likharev, K. K. *Mesoscopic Phenomena in Solids*; Altshuler, B. L., Lee, P. A., Webb, R. A., Eds.; Elseveir: Amsterdam, 1991; p 169.
(20) Hanna, A. E.; Tinkham, M. *Phys. Rev. B: Condens. Matter Mater. Phys.* **1991**, *44*, 5919−5922.
(21) Taniguchi, T.; Watanabe, K. *J. Cryst. Growth* **2007**, *303*, 525−529.
(22) Alem, N.; Yazyev, O. V.; Kisielowski, C.; Denes, P.; Dahmen, U.; Hartel, P.; Haider, M.; Bischoff, M.; Jiang, B.; Louie, S. G.; Zettl, A. *Phys. Rev. Lett.* **2011**, *106*, 126102.
(23) Jin, C.; Lin, F.; Suenaga, K.; Iijima, S. *Phys. Rev. Lett.* **2009**, *102*, 195505.
(24) Ju, L.; Velasco, J., Jr; Huang, E.; Kahn, S.; Nosiglia, C.; Tsai, H. J.-Z.; Yang, W.; Taniguchi, T.; Watanabe, W.; Zhang, Y.; Zhang, G.; Crommie, M.; Zettl, A.; Wang, F. *Nat. Nanotechnol.* **2014**, *9*, 348−352.
(25) Wong, D.; Velasco, J., Jr.; Ju, L.; Lee, J.; Kahn, S.; Tsai, H.-Z.; Germany, C.; Taniguchi, T.; Waranabe, K.; Zettl, A.; Wanf, F.; Crommie, M. arXiv:1412.1878, 2014.
(26) Dean, C. R.; Young, A. F.; Meric, I.; Lee, C.; Wang, L.; Sorgenfrei, S.; Watanabe, K.; Taniguchi, T.; Kim, P.; Shepard, K. L.; Hone, J. *Nat. Nanotechnol.* **2010**, *5*, 722−726.
(27) Zobelli, A.; Ewels, C. P.; Gloter, A.; Seifert, G. *Phys. Rev. B: Condens. Matter Mater. Phys.* **2007**, *75*, 094104.
(28) Wang, J.; Li, S. N.; Liu, J. B. *J. Phys. Chem. A* **2015**, *119*, 3621−3627.

DOI: 10.1021/acs.nanolett.5b02625
Nano Lett. 2015, 15, 7329−7333